
This is an electronic reprint of the original article.
This reprint may differ from the original in pagination and typographic detail.

Stekrova, Martina; Rinta-Paavola, Aleks; Karinen, Reetta

Hydrogen production via aqueous-phase reforming of methanol over nickel modified Ce, Zr and La oxide supports

Published in:
Catalysis Today

DOI:
[10.1016/j.cattod.2017.08.030](https://doi.org/10.1016/j.cattod.2017.08.030)

Published: 01/04/2018

Document Version
Peer-reviewed accepted author manuscript, also known as Final accepted manuscript or Post-print

Published under the following license:
CC BY-NC-ND

Please cite the original version:
Stekrova, M., Rinta-Paavola, A., & Karinen, R. (2018). Hydrogen production via aqueous-phase reforming of methanol over nickel modified Ce, Zr and La oxide supports. *Catalysis Today*, 304, 143-152.
<https://doi.org/10.1016/j.cattod.2017.08.030>

This material is protected by copyright and other intellectual property rights, and duplication or sale of all or part of any of the repository collections is not permitted, except that material may be duplicated by you for your research use or educational purposes in electronic or print form. You must obtain permission for any other use. Electronic or print copies may not be offered, whether for sale or otherwise to anyone who is not an authorised user.

Hydrogen production via aqueous-phase reforming of methanol over nickel modified Ce, Zr and La oxide supports

Martina Stekrova*, Aleksi Rinta-Paavola, Reetta Karinen

Department of Chemical and Metallurgical Engineering, Aalto University, Kemistintie 1, 02150 Espoo, Finland

**Corresponding author: martina.stekrova@aalto.fi, Kemistintie 1, 02150 Espoo, Finland*

Keywords: aqueous-phase reforming; methanol; nickel-based catalyst; zirconium, cerium and lanthanum mixed oxides

Abstract

Aqueous-phase reforming (APR) of methanol over nickel supported on zirconium, cerium and lanthanum oxides was performed in continuous laboratory scale reactor and discussed in this paper. The role of composition and physico-chemical properties of the supports were investigated and significant benefit of using mixed oxides $\text{CeO}_2\text{-ZrO}_2$ and $\text{La}_2\text{O}_3\text{-ZrO}_2$ over the pure oxides, in term of methanol conversion and hydrogen production, was demonstrated. Methanol conversion of over 50 % with hydrogen production efficiency of over 40 % were achieved with the most active catalyst $\text{Ni}/25\%\text{CeO}_2\text{-ZrO}_2$.

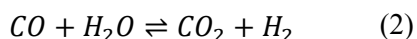
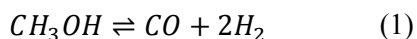
Furthermore, catalyst stability, the most challenging issue within APR studies, was thoroughly investigated and discussed. Slight deactivation of the prepared catalysts during APR experiments or reduction was observed and addressed to the Ni particles sintering. On the other hand, other common reasons causing catalysts deactivation under APR conditions, such as leaching of Ni, changes in Ni oxidation state or changes in the supports lattice were not observed by wide range of characterization methods. The most stable catalyst, $\text{Ni}/10\%\text{La}_2\text{O}_3\text{-ZrO}_2$, exhibited a slight decrease of MeOH conversion within two subsequent experiments (each per 6h) from 46.3 % to 42.7 %.

1. Introduction

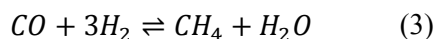
Aqueous-phase reforming (APR) is a promising technology converting organic compounds in aqueous solutions preferably to hydrogen and carbon dioxide. Therefore, APR can be considered as a potential route for transformation of organic compounds found in biorefinery wastewaters to value added products. This would lead to increasing economic efficiency of processes such as biomass pyrolysis and Fischer-Tropsch synthesis and make them more environmentally friendly by decreasing the amount of organic compounds in wastewater streams. In comparison with well-known steam reforming, APR has proven to be more energy efficient because of no need of evaporating feedstock to gas phase [1].

Very challenging task within the research focused on APR has been the finding of a suitable catalyst, which would show high activity in reforming reaction (Eq. 1) and water-gas shift (WGS, Eq. 2) reaction and remain stable under the demanding APR reaction conditions. Furthermore, the catalyst should not support the cleavage of C-O bonds and hydrogenation of CO and CO₂ should be suppressed (e.g. Eqs. 3 and 4).

Desired reactions



Undesired reactions



In general, Group VIII metals exhibit high activity for C-C bond scission. The highest activity and hydrogen selectivity in reforming reactions have typically been achieved over Pt-based catalysts, especially Pt supported on γ -Al₂O₃ [2–4]. However, comparable activities were achieved over cheaper nickel catalysts [5]. Nickel supported catalysts have generally shown high conversion and high hydrogen selectivity [5]. However, the most tested nickel-based catalysts deactivated rapidly, due to the changing of the oxidation state of Ni, sintering or structural changes of the support [6]. Therefore, supports based on ZrO₂ and CeO₂ were selected to be tested as a potentially stable supports for Ni in the current paper.

Zirconium and cerium oxides are used extensively as catalyst supports in various applications [7–9]. Zirconium oxide may act as a catalyst itself, for example in alkene isomerization, alcohol dehydration and in many petrochemical processes, such as hydrocarbon hydrogenation, dehydrogenation or cracking. As a catalyst support, zirconia has been employed in CO oxidation and water-gas shift reaction [8]. Ceria based catalysts are used in automotive exhaust catalysts, in fluid catalytic cracking and oxidation of volatile organic compounds [7]. The most important property of cerium oxide as a catalyst support is its oxygen storage capacity and oxygen mobility throughout the lattice, which promotes catalysts activity mainly in WGS reaction [10,11]. This property also efficiently suppresses the formation of carbon deposits on the catalyst surface [12,13] which is, however, most likely not an issue in APR [3]. Especially, mixed oxides of ceria and zirconia have many advantages over pure oxides, such as high stability, resistance towards coking and high oxygen storage capacity [9].

Doping cerium oxide with a lower-valence metal, such as lanthanum, leads to increase of oxygen mobility and oxygen storage capacity via the formation of oxygen vacancies. In case of pure zirconia, lanthanum doping leads to stabilizing of the oxide lattice [14] and causes stronger metal-support interaction, which is beneficial for producing highly dispersed Ni species and avoiding particle coalescence [15–19].

Platinum modified mixed oxides of CeO₂ and ZrO₂ have been studied in APR reaction of glycerol [20,21]. Effect of Ce/Zr ratio has been found out to affect Pt oxidation state, metal dispersion and surface area, and particle size [20]. In another study, Pt supported on Ce-Zr mixed oxides have been successfully applied for APR of the low-boiling fraction of bio-oil and additionally, catalyst recyclability by calcination was proven [22]. Enhanced activity and stability in APR of ethylene glycol was achieved by using Co as promoter to Pt/CeO₂-ZrO₂ [23]. Platinum-rhenium synergy on zirconia, ceria and their mixed oxides have been evaluated by Ciftci et al. [21] in APR of glycerol.

In addition to platinum catalysts, Ni supported on mixed oxides such as LaAlO₃, CeO₂ and MgO has been employed in APR of glycerol resulting in high activity and catalyst stability [24]. Activity of Ni/CeO₂ was evaluated in APR of ethanol [12] and *n*-butanol [25] and showed higher efficiency and H₂ and CO₂ selectivity compared to Ni/Al₂O₃. Bimetallic Pt-Ni composites on ceria-doped alumina supports have been studied in APR of glycerol targeting to minimize amount of expensive Pt [26]. Mono- and bi-metallic catalyst of Ni and Pt supported on mesoporous zirconium oxide as well as on ceria-zirconia-silica supports in APR of sorbitol have been tested and significant differences in the catalysts reducibility and consequent activity have been revealed by Tanksale et al. [27].

The main target of the current investigation is to study the application of APR process in the treatment of biorefinery wastewaters. Based on the typical compositions of wastewaters originating from Fischer-Tropsch process as well as of biomass pyrolysis water streams [28,29], methanol was selected as a model compound. Biorefinery wastewaters contain mixture of wide range of chemical compounds and among them methanol is the only compound that can be found in high concentrations in all types of wastewaters. Even though methanol is not a typical feedstock for APR studies, since the catalyst activity in C-C cleavage cannot be evaluated, its reforming will be crucial in case of studying the potential of utilizing APR process in larger scale.

2. Experimental

2.1 Materials

Granulated zirconium dioxide supplied by Saint-Gobain Ceramic Materials was calcined at 500 °C in air for 10 h. Cerium(IV) oxide supplied by Sigma-Aldrich (99.9 %) was calcined at 450 °C in air for 10 h. Zirconium, cerium and lanthanum mixed oxides (17 wt-%CeO₂-ZrO₂, 25 wt-%CeO₂-ZrO₂, 17 wt-%CeO₂-5 wt-%La₂O₃-ZrO₂, 10 wt-%La₂O₃-ZrO₂) were supplied by MEL Chemicals in amorphous form and calcined at 450 °C in air for 10 h to obtain the desired oxide forms. Before metal modifications, all supports were first pelletized, then crushed, and sieved in order to obtain particles with well-defined particle size suitable for placing on sinter of fixed bed tubular reactor (particle diameter of 200 – 300 μm). Nickel nitrate (Ni(NO₃)₂·6H₂O, ≥97.0 %) utilized as the metal precursor was supplied by Sigma-Aldrich.

2.2 Catalysts preparation

Zirconia, ceria and lanthanum oxide and their mixtures (ZrO_2 , 17% CeO_2 - ZrO_2 , 25% CeO_2 - ZrO_2 , 17% CeO_2 -5% La_2O_3 - ZrO_2 , 10% La_2O_3 - ZrO_2 and CeO_2) were used as the supports for nickel (10 wt-%) modified catalysts. Metal modification of the supports was performed using conventional incipient wetness impregnation method. The support material was mixed with aqueous solution of nickel nitrate and kept for 24 hours at room temperature, followed by drying at 110 °C and calcination at 500 °C for 4 h under air flow. Reduction of the catalyst was performed *in situ* in APR reactor before each experiment (reduction conditions: 450 °C, 25 bar, $\text{N}_2 = \text{H}_2 = 5$ l/h, 2 h).

2.3 Catalysts characterization

Wide range of characterization methods such as atomic absorption spectroscopy (AAS), nitrogen adsorption and desorption (BET and BJH method), high-resolution transmission electron microscope (HR-TEM), X-ray diffraction (XRD), were used for describing the properties of the prepared catalysts.

The metal loading of the prepared catalysts was analyzed using atomic absorption spectroscopy (AAS). 200 mg of sample was dissolved in closed teflon vessels with HNO_3 and HCl at 120 °C. After cooling, the sample was diluted with Milli-Q water. Varian AA240 AAS equipment using air-acetylene flame was used for the determination of Ni loading.

Nitrogen physisorption (Ultra Surfer, Thermo Fisher) was used to determine surface area, pore volume, and pore size distribution of the pure supports and the prepared catalysts. The degassing of the samples was performed prior to the measurement under vacuum for 3 h at 200 °C. In the case of the spent catalysts, the degassing of samples was performed under vacuum at 120 °C for 5 h in order to prevent desorption of the compounds potentially adsorbed during the APR experiments. Surface areas were calculated using BET method and pore volumes as well as pore diameters by BJH method from nitrogen desorption isotherms.

Hydrogen static volumetric chemisorption (Ultra Surfer, Thermo Fisher) was used to determine nickel dispersion and its surface area. The catalyst was reduced at 450 °C in H_2 flow (15 ml/min) for 2 h and then degassed at the same temperature under vacuum for 2 h prior to the measurement. Hydrogen chemisorption was performed at room temperature.

The type of the surface species on the catalyst was determined by X-ray diffraction (XRD) analysis using PANalytical X'Pert PRO MPD Alpha-1 diffractometer with $\text{Cu K}\alpha 1$ radiation (45 kV and 40 mA). If needed, the sample was ground before placing it into the sample holder prior to the analysis. The X-ray scanning was performed in continuous scan mode in the range of 10 - 90° (2θ) and a step size of 0.0131°. The mean metal crystallite diameter was estimated for some of the catalysts using the Scherrer equation based on the peak broadening of the most intense peaks.

An aberration-corrected JEOL-2200FS microscope (JEOL Ltd., Japan), operated at 200 kV was used for scanning transmission electron microscopy (STEM). Particle size of the supports were evaluated using Gatan DigitalMicrograph software. The EDS analysis was applied for the chemical characterization of the selected samples and recording of elemental maps.

The CO_2 temperature-programmed desorption (CO_2 -TPD) was carried out in an Altamira Instruments AMI-200R flow-through set-up equipped with Hiden QIC-20 mass spectrometer for outlet gas analysis. 100 mg

of support was placed in a quartz U-tube and pretreated in 20% O₂/He (flow 20 ml/min) at 600 °C (heating rate 15 °C/min) for 2 h. Thereafter the sample was cooled down to adsorption temperature ($T_{ads} = 40$ or 100 °C) in flowing He. The adsorption was performed by feeding 500 μ L pulses of CO₂ to the He flow at 4-minute interval. After adsorption the sample was flushed for 10 min with He and then heated at a constant rate of 15 °C/min up to 600 °C and held there for 10 min to ensure full desorption of CO₂.

2.4 Catalytic activity tests

APR experiments were performed in a continuously operated stainless steel tubular reactor using downward flow. The catalyst (1.5 g) was loaded on a sinter placed in the midsection of the reactor with 15 mm of inner diameter. Reaction conditions of experiments were 230 °C and 32 bars. A 5 wt-% aqueous solution of methanol was fed to the reactor using HPLC pump with a flow of 120 ml/h. In addition, N₂ was fed through the reactor with flow of 4.5 l/h during the whole experiment and its flow was used as an internal standard for evaluating the composition of gaseous product.

The outlet stream from the reactor was cooled down and separated into gas and liquid phases at the reactor pressure. The gaseous products were analysed online by MicroGC (Agilent 490 Micro GC Biogas Analyzer) consisting of a dual channel cabinet including a 10-meter CP-Molsieve 5A with argon as carrier gas, and a 10-meter CP-PoraPLOT U column channel with helium carrier gas and equipped with 2 thermal conductivity detectors (TCD).

The liquid products were taken at specific time intervals and analysed offline by a gas chromatograph (Agilent 6890 series) equipped with a flame ionization detector (FID) and a Zebtron ZB-wax Plus column (60 m x 0.25 mm x 0.25 μ m). Butan-2-ol was used as an external standard.

After the experiment, the catalyst was kept in the reactor, re-reduced using the same reduction condition as in the case of fresh catalyst and tested again in a subsequent APR experiment under the same reaction conditions. After the second experiment, the spent catalyst was characterized in order to determine reasons for potential deactivation.

The results of the catalyst screening in APR were evaluated in terms of hydrogen production efficiency (E_{H_2} , Eq. 5), total conversion of methanol (X , Supplementary material Eq. S1), hydrogen production rate (r_{H_2} , Supplementary material Eq. S2), product yields (Y_i , Supplementary material Eq. S3) and product selectivities (S_i , Supplementary material Eq. S4).

$$E_{H_2}(\%) = \frac{\dot{n}_{out}^{H_2}}{\dot{n}_{max}^{H_2}} \times 100 \quad (5)$$

Where $\dot{n}_{out}^{H_2}$ (μ mol/min) is molar flow rate of H₂ in gaseous product and $\dot{n}_{max}^{H_2}$ (μ mol/min) is theoretical maximal H₂ production (being 3 μ mol/min from 1 μ mol/min of MeOH).

3. Results and discussion

3.1 Catalyst characterization

Deep characterization of all prepared catalysts, namely Ni/Zr (10%Ni/ZrO₂), Ni/17Ce-Zr (10%Ni/17%CeO₂-ZrO₂), Ni/25Ce-Zr (10%Ni/25%CeO₂-ZrO₂), Ni/17Ce-5La-Zr (10%Ni/17%CeO₂-5%La₂O₃-ZrO₂), Ni/10La-Zr (10%Ni/10%La₂O₃-ZrO₂), and Ni/Ce (10%Ni/CeO₂), revealed differences in pore size, surface areas, and metal particle size.

3.1.1 Quantitative analyses by atomic absorption spectroscopy (AAS)

Ni content in fresh and spent catalysts detected using AAS method is shown in Table 1. As the consequence of the preparation method, the success of Ni deposition on various supports was above 90 % of the nominal loading as the content of 10 wt-% of Ni was targeted in each case. The small differences in Ni content are addressed to measurement error. As can be seen by comparing the Ni content of fresh and spent catalysts, Ni was leached slightly (below 1 % point of Ni after 12 h on stream) from pure ZrO₂, CeO₂ and support 17Ce-5La-Zr during the experiments.. On the other hand, no Ni leaching was observed after two APR experiments from either Ce-Zr or La-Zr supports. These results revealed that Ni leaching cannot be decisive reason for catalyst deactivation under APR conditions and the contribution of homogeneous catalysis by leached Ni can be neglected as the experiments were performed in continuous flow mode.

Table 1. Ni content in fresh and spent catalyst determined using AAS.

Catalyst	Ni content (wt-%)	
	Fresh	Spent
Zr	9.4	8.6
17Ce-Zr	9.5	9.7
25Ce-Zr	9.3	9.2
17Ce-5La-Zr	10.1	9.3
10La-Zr	9.0	9.0
Ce	9.2	8.3

3.1.2 Textural properties by nitrogen adsorption-desorption

The textural characteristics of pure supports and Ni-modified catalysts (fresh and spent) are shown in Table 2. Surface area of the supports differed significantly ranging from very low (9.9 m²/g) in case of pure CeO₂ to relatively high (136.1 m²/g) in case of 17Ce-5La-Zr.

The surface areas and pore volumes (Table 2) of all tested supports decreased with Ni impregnation, which was caused by the partial blockage of some pore entrances by the metal particles. The value of average pore diameter increased in the most cases after Ni loading. This fact was explained by blocking of the smallest pores by Ni particles either after metal loading or by Ni particles sintering during the APR experiments. Decrease in volume of micropores which leads to the higher calculated pore diameter is presented in Supplementary material (Section S2.) comparing the total pore volumes and volumes of micro-, meso- and macropores (Supplementary material, Table S1). In addition, pore size distribution of all supports and their Ni modified forms (fresh and spent) are shown in Supplementary material (Fig. S1, Section S2.).

Negligible differences in surface areas and pore volumes were observed in case of spent Ni/Zr, Ni/17Ce-Zr, Ni/25Ce-Zr and Ni/10La-Zr. However, significant decrease of surface area was observed in case of spent Ni/17Ce-5La-Zr compared to the fresh catalyst. This material (pure support and Ni modified catalyst) exhibited the highest surface areas and pore volumes as well as the smallest average pore diameters. Therefore, the blockage of the smallest pores by Ni particles sintering led to the most significant differences in measured values between fresh and spent catalyst (see below Section 3.1.4). Significant decrease in surface area was also determined for spent Ni/Ce. This decrease is attributed to the proven formation of carbonates on surface of this catalyst (see below Section 3.1.4).

Table 2. Textural properties of pure supports, and Ni modified fresh and spent catalysts.

Catalyst or support		Specific surface area (m²/g)	Pore volume (cm³/g)	Average pore diameter (nm)
Zr	-	97.6	0.32	8.4
	10 %	59.7	0.26	11.7
	spent	62.1	0.27	13.4
17Ce-Zr	-	112.0	0.22	7.0
	10 %	73.3	0.20	8.5
	spent	72.3	0.20	8.6
25Ce-Zr	-	98.8	0.28	10.7
	10 %	82.7	0.26	10.9
	spent	75.5	0.29	11.4
17Ce-5La-Zr	-	136.1	0.37	3.6
	10 %	114.0	0.36	3.7
	spent	84.8	0.29	6.0
10La-Zr	-	78.9	0.31	14.7
	10 %	68.7	0.25	12.6
	spent	64.5	0.25	14.0
Ce	-	9.9	0.07	2.8
	10 %	7.2	0.05	2.6
	spent	3.9	0.02	3.7

The N₂ adsorption-desorption isotherms of all tested materials are shown in Fig. 1. Zirconium oxide and all mixed oxides and their Ni modified forms were characterized by isotherms type IV (according to IUPAC classification) with a H₂-type hysteresis loop, typical for mesoporous materials. As can be seen from the isotherms, these materials contain negligible amount of micropores in their structure (See also Supplementary material, Table S1).

On the contrary, CeO₂ was characterized by nonporous structure which can be seen from its isotherm type III (IUPAC classification) and which results in very low surface area of this material.

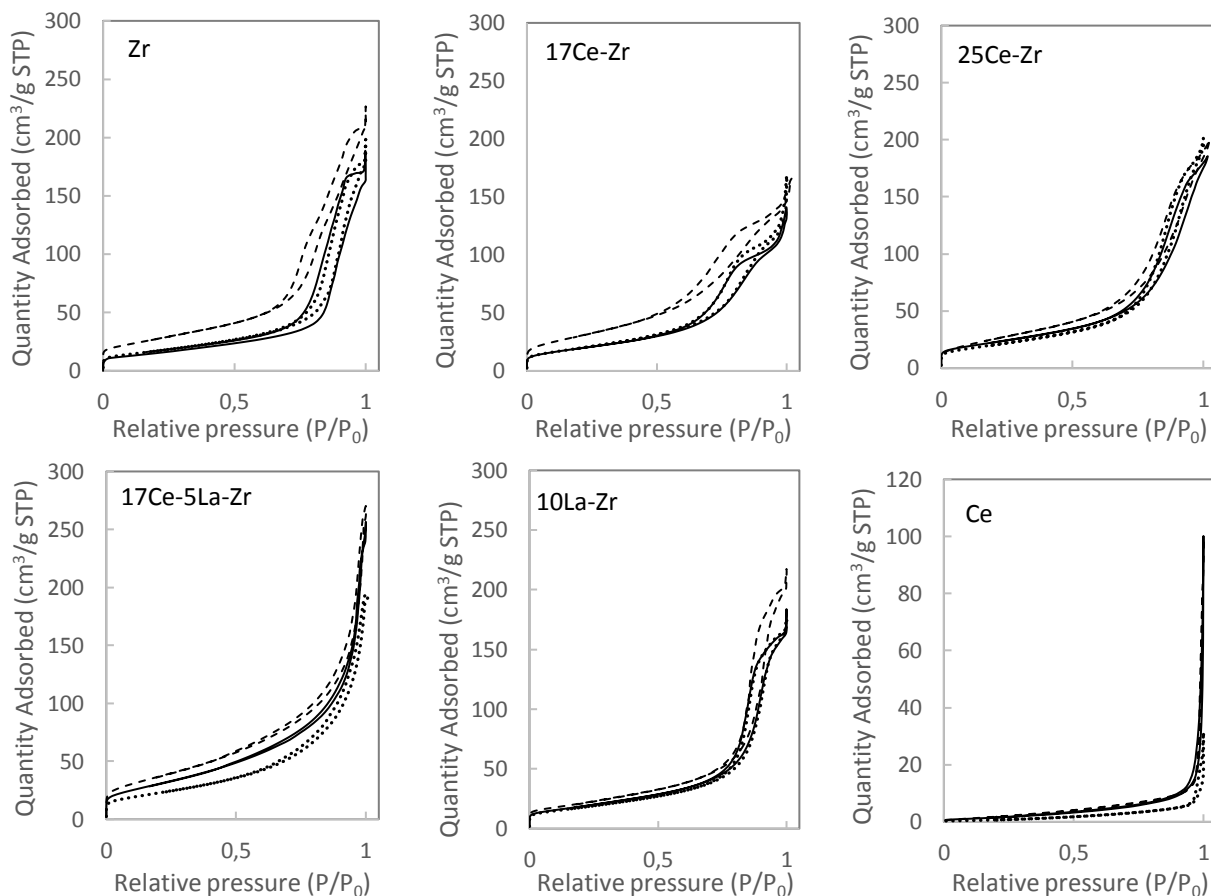


Figure 1. Isotherms of pure supports (dashed line), 10% Ni modified materials (line) and spent catalyst (dots).

3.1.3 Hydrogen chemisorption

In order to determine an accessible Ni surface and dispersion, H₂ chemisorption was performed for all tested fresh catalysts (Table 3). Ni dispersion in range of 3-6 % was determined on all supports in exception of Ni/Ce. As mentioned, CeO₂ exhibited nonporous character with very low surface area and therefore, higher dispersion of Ni cannot be reached.

As discussed below, larger Ni particles were determined using H₂ chemisorption than XRD line-broadening (See Section 3.1.4 and Table 5) which could be a consequence of Ni particles sintering during the reduction step. It should be noted here, that the reduction of catalysts prior to the chemisorption analyses was performed at atmospheric pressure and 450 °C for 2 h while the reduction performed *in situ* prior to the APR experiment was done at 25 bar and the same temperature and time. Therefore, it is not possible to estimate, real Ni particles size on the catalysts tested in APR experiments.

Table 3. Ni dispersion, particle size and surface area determined by H₂ chemisorption.

Catalyst	Ni dispersion (%)	Ni particle size (nm)	Ni surface area (m ² /g)
Zr	3.9	26.0	25.9
17Ce-Zr	5.8	17.4	38.7
25Ce-Zr	3.7	27.3	24.7
17Ce-5La-Zr	2.9	35.6	19.1
10La-Zr	4.6	21.9	30.7
Ce	<i>n.a.</i>	<i>n.a.</i>	<i>n.a.</i>

n.a. = not available

3.1.4 Structural analysis by X-ray diffractometer (XRD)

XRD patterns of the pure supports and their Ni modified forms are presented in Fig. 2. The characteristic monoclinic phase (JCPDS card number 13-307) for ZrO₂ was identified in pure and Ni modified zirconia. XRD pattern of CeO₂ exhibited main reflections on the 2θ scale 28.5°, 33.0°, 47.5°, 56.4°, 59.1°, 69.4°, 76.7°, 79.1° and 88.4° corresponding to (111), (200), (220), (311), (222), (400), (331), (420) and (422) planes, respectively, which are characteristic of the cubic ceria phase with fluorite structure (JCPDS card number 34-394) [30,31]. Patterns of all mixed oxides were very similar to each other showing the absence of phases typical for pure oxides and low crystallinity of these materials.

Nickel oxide is typically characterized by the five diffraction peaks listed in Table 4. Among those, four diffraction peaks were observed in the XRD patterns of all prepared catalysts (Fig. 2).

Table 4. The dominant peaks of NiO and metallic Ni available in the measured range [32,33].

Phase	Position (2θ)	Reflections [h k l]	Phase	Position (2θ)	Reflections [h k l]
NiO	37.3	1 1 1	Ni	44.3	1 1 1
	43.3	2 0 0		51.7	2 0 0
	62.9	2 2 0		76.2	2 2 0
	75.4	3 1 1			
	79.4	2 2 2			

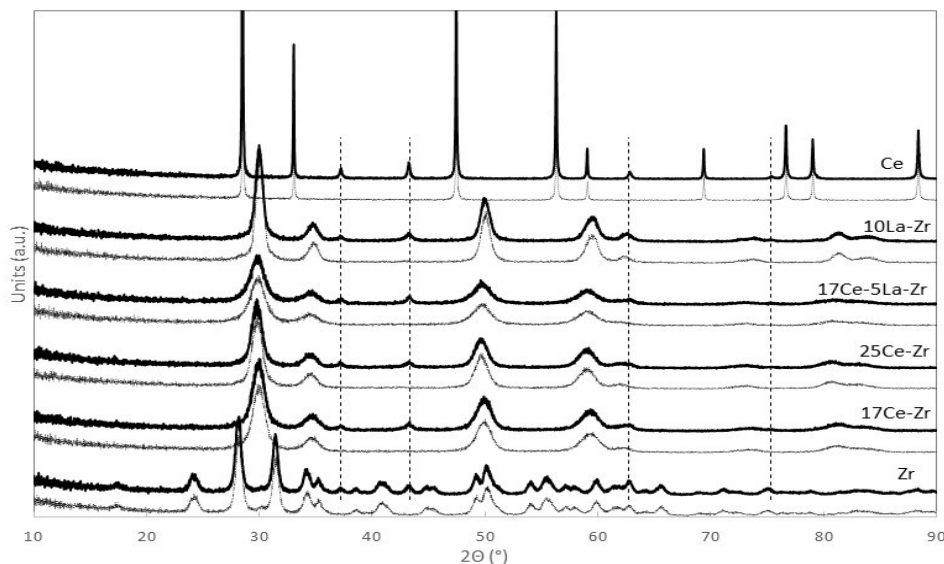
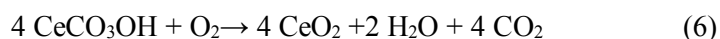


Figure 2. XRD patterns of the pure supports (thin line) and Ni modified catalysts (thick line) with marked NiO characteristic peaks.

XRD patterns of the spent catalysts are shown in Supplementary material (Fig. S2, Section S3.). XRD patterns typical for all supports, in exception of CeO₂, remained the same showing no changes in the oxides lattice during the APR experiments (See also Table 5). Metallic Ni is typically characterized by the three diffraction peaks (listed in Table 4) which all were visible in the XRD patterns of all spent catalysts. No peaks characteristic for NiO were present in any of the spent catalysts suggesting that the total reduction of metal species was reached by *in situ* reduction performed before experiment and no oxidation of metallic Ni took place during the APR experiments.

XRD pattern of spent Ni supported on CeO₂ contained peaks typical for cubic cerium dioxide phase but also peaks typical for hexagonal cerium carbonate hydroxide (CeCO₃OH) (marked with ○ in Supplementary material (Fig. S2, Section S3.)). Formation of carbonates during WGS reaction over CeO₂ supported catalysts has been previously confirmed by *in situ* DRIFTS studies using different metal modified CeO₂ [34]. It has been claimed that CO adsorbed on active metal species reacts with OH groups originating from dissociated water on the catalysts surface, to generate formate intermediates or formic acid (HCOOH). The formates react further with water, producing hydrogen and carbonates, which in the final step decompose to generate CO₂ [34–36]. Formation of formates and carbonates has been found out to be main reason for catalysts deactivation in WGS. However, the catalytic activity could be fully recovered by the calcination of the deactivated materials in air at elevated temperatures [36]. Carbonate thermal decomposition toward CeO₂ was reached within 1 h at 300 °C in flowing air as shown in Eq. 6 [37].



However, the deactivation of Ni/CeO₂ was not investigated in the present research because of its very low initial activity; thus, the re-activation of this material was not studied.

XRD line-broadening and Scherrer equation were used to estimate the crystal size of NiO and metallic Ni in fresh and spent catalysts, respectively (Table 5). Crystal sizes present on fresh and spent catalysts were determined using the most intensive peaks being $43.3^\circ 2\theta$ for NiO and $44.4^\circ 2\theta$ for metallic Ni.

Crystallites of NiO, being in the range from 11 to 13 nm, were determined on all supports in exception of CeO₂ where Ni particles formed bigger clusters (over 30 nm) in accordance to its very low surface area (9.9 m²/g).

As mentioned above (Section 3.1.3), smaller crystallites of NiO were determined using XRD line-broadening than using H₂ chemisorption (Table 3). On the other hand, the trend of the sizes is in line using both methods. The chemisorption measurement was performed on the reduced catalysts while XRD patterns were recorded for calcined materials. Therefore, the differences between those two methods could suggest metal particles sintering during the reduction step. Particle growth during reduction step has been observed by Manfro et al. [38].

Comparison of NiO crystal size present on fresh catalyst and Ni crystal size present on spent catalysts (Table 5), suggests significant sintering of Ni under APR conditions. It should be noted here, that Ni/Ce was used only in one APR experiment while all the other catalysts were characterized after testing in two subsequent APR experiments. Very significant sintering was observed in case of pure ZrO₂ and all supports containing Ce, where Ni crystallites on the spent catalysts were at least 4 times larger than NiO crystals on the fresh ones. It should be emphasized that even though it has been published previously that compared to pure oxide support, strong interaction exists between the mixed oxide supports and metal [39], Ni sintering in the current study was comparable in case of using pure zirconia as well as mixed oxide supports containing CeO₂ in the lattice.

On the other hand, lower sintering was determined in case of Ni supported on 10La-Zr mixed oxide lattice. This can be consequence of strong interaction of between Ni and La₂O₃ which was described to be effective in inhibiting the migration of Ni and carbon deposition [18,19].

In addition to the determination of the crystallite size of the active metal, XRD line-broadening and Scherrer equation were used to determine the crystal size of the oxides in the pure supports as well as in the Ni modified fresh and spent catalysts (Table 5). As mentioned above, no significant changes in the oxides lattice were observed neither after nickel loading nor during the APR experiments and the crystallite sizes for all supports remained comparable. The dimensions of mixed oxides crystallites containing Ce in the lattice were in the range of 5.1-7.2 nm, whereas they were slightly larger in the case of La-Zr support being 9.5 nm. In contrast, ZrO₂ and CeO₂ were characterized by larger crystallite sizes. Smaller crystallites of mixed oxides of Ce and Zr can be attributed to the incorporation of the small-size zirconium species into the matrix of CeO₂ as has been previously described by Jeon et al. [40]. Smaller crystallites in case of 10La-Zr comparing to pure ZrO₂ can be explained correspondingly.

Table 5. Ni species and supports oxides crystal size measured by XRD.

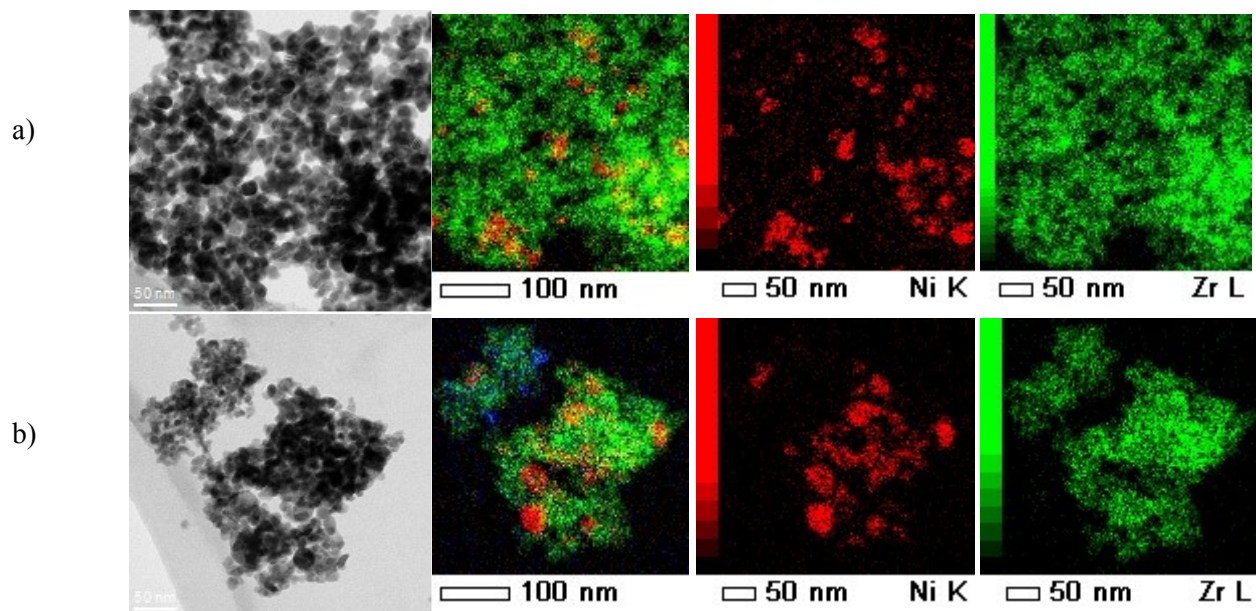
Catalyst	Crystallite size of Ni species (nm)	Crystallite size of oxides (nm)
----------	-------------------------------------	---------------------------------

	d_{NiO} (FRESH)	d_{Ni} (SPENT)	Pure support	FRESH catalyst	SPENT catalyst
Zr	12.7	47.6	13.9	15.2	15.2
17Ce-Zr	11.3	48.5	6.4	6.5	6.7
25Ce-Zr	12.9	48.8	7.2	6.9	6.6
17Ce-5La-Zr	13.1	46.4	5.1	5.1	6.4
10La-Zr	12.2	33.9	9.5	9.3	9.5
Ce	33.8	61.5	74.5	82.9	73.8

3.1.5 Transmission electron microscopy (HR-TEM and STEM)

The selected nickel-modified catalysts were characterized by TEM in order to determine the nickel particle size, morphology, and their distribution on the catalyst surface (Fig. 3, bright field STEM images).

Because of the fact that elements present in the supports (Zr, Ce, La) are heavier than Ni, it was not possible to see metal particles using neither HR-TEM, nor STEM. Therefore, the elemental maps determining the location of the elements were recorded and they are presented in Fig. 3, showing location of Ni (red), location of Zr (green) and their overlay (blue color is dedicated to Ce in case of Ni/17Ce-Zr in Fig. 3b and to La in case of Ni/10La-Zr in Fig. 3c). As can be seen from the elemental maps, Ni is not equally distributed on any of those supports, showing that Ni particles are present most probably in forms of larger agglomerates.



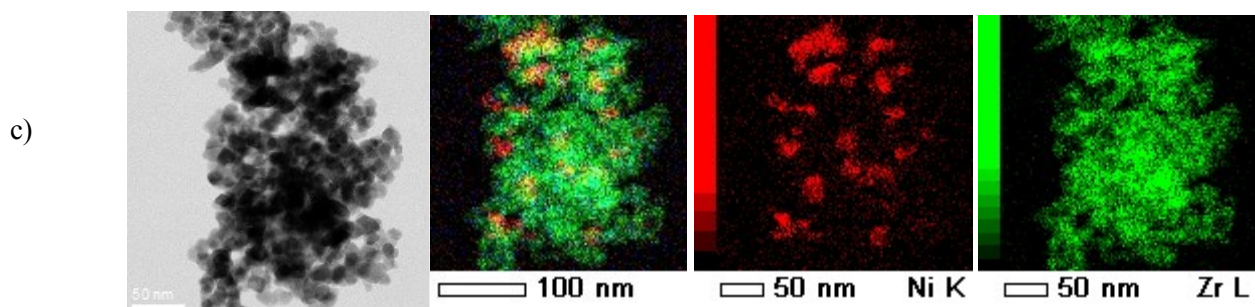


Figure 3. TEM micrographs, and the elemental maps recorded by EDS of Ni catalysts: (a) Ni/Zr, (b) Ni/17Ce-Zr and (c) Ni/10La-Zr.

3.1.6 Temperature-programmed desorption (CO_2 -TPD)

Temperature-programmed desorption of CO_2 (CO_2 adsorbed at 40 and 100 °C) was performed to characterize the basicity of the supports. The CO_2 -TPD profiles (CO_2 adsorption at 100 °C) are shown in Fig. 4 and amounts of desorbed CO_2 for both adsorption temperatures are given in Table 6.

One broad CO_2 desorption maximum with T_{max} being ca. 200 °C, can be seen in the TPD profiles of the supports containing Ce in their lattice (17Ce-Zr, 25Ce-Zr and 17Ce-5La-Zr). In contrast, CO_2 -TPD profile of pure ZrO_2 shows two maxima at 200 °C and 330 °C. A different trend can be seen in the TPD profile of 10La-Zr, exhibiting a broad distribution of basic sites over the temperature range of 200-550 °C.

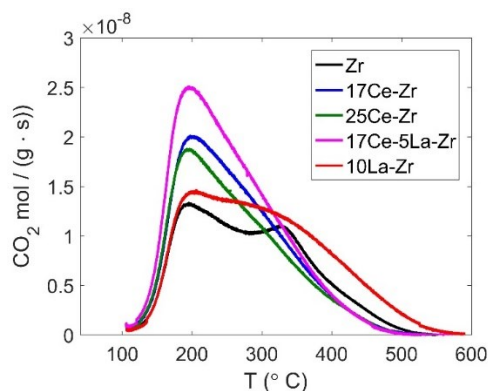


Figure 4. TPD profiles of CO_2 adsorbed at 100 °C for the Zr-based supports.

Desorbed CO_2 amounts after adsorption at 40 °C results in the total amount of basic surface sites (weak and strong sites) while desorbed CO_2 amounts after adsorption at 100 °C represent the stronger basic sites. Doping pure ZrO_2 with either CeO_2 or La_2O_3 increased the amount of total basic surface sites (CO_2 adsorption at 40 °C in Table 6). The highest amount of desorbed CO_2 at both adsorption temperatures was obtained with 17Ce-5La-Zr catalyst indicating the highest amount of both weak and stronger basic sites. Since Garcia et al. have reported that nickel impregnation on ZrO_2 did not affect the amount of basic sites on the catalyst [41], it is therefore assumed that the basic nature of the prepared Ni catalysts is similar to that of the supports.

Table 6. Desorbed CO_2 amounts from the supports in TPD performed up to 600 °C.

Catalyst	Desorbed CO ₂ (μmol/g)	
	T _{ads} = 40 °C	T _{ads} = 100 °C
Zr	130	100
17Ce-Zr	180	130
25Ce-Zr	170	120
17Ce-5La-Zr	200	150
10La-Zr	170	140
Ce	<i>n.a.</i>	<i>n.a.</i>

3.2 Catalytic activity tests

All prepared catalysts were tested in APR of methanol aqueous solution under the same reaction conditions (See Section 2.4). In addition, blank test with the pure support 17Ce-5La-Zr was performed and negligible conversion of methanol (below 1 %) was detected with no production of any gaseous products indicating that the catalytic activity can be attributed to Ni.

Hydrogen, methane, CO and CO₂ were detected as the main gaseous products. Furthermore, ethane and propene were detected in negligible amounts (up to 0.1 %). Only unconverted methanol was detected in the liquid samples and its concentration was used to determine its conversion. Carbon balance for all experiments was calculated to be around 90 % indicating the ratio of analyzed carbon to the carbon in the feed. The missing carbon most probably remained in aqueous phase as dissolved CO₂ because of the gas-liquid separation performed at elevated pressure (32 bar) and therefore the calculated yield of CO₂ is probably slightly lower than the real yield.

Table 7 compares achieved methanol conversions, hydrogen production efficiencies and selectivities towards gaseous products achieved over all tested catalysts in the steady state (achieved within 90 min from the beginning of the reaction) (See Fig. 6). The prepared catalysts showed relatively high activities in APR of methanol with the highest conversions being over 50 % achieved over Ni on both supports containing CeO₂ and ZrO₂ (17Ce-Zr and 25Ce-Zr). High and comparable conversion of MeOH being around 46 % were also achieved over both supports containing La in their lattice (17Ce-5La-Zr and 10La-Zr). On the other hand, the lowest activity in APR and the lowest H₂ yield was achieved when pure CeO₂ was applied as a support probably due to the low surface area and very poor metal dispersion. Lower activity was achieved also over Ni/ZrO₂ which indicates that the use of mixed oxides is highly beneficial.

As a contrast, Ciftci et al. [21] has reported higher activity achieved over Pt supported on pure ZrO₂ than on CeZrO₂ in APR of glycerol, whereas the opposite trend has been determined for the bimetallic catalysts of Pt and Re on these supports. The overall order of activity in glycerol APR using those supports has been PtRe/CeZrO₂>PtRe/ZrO₂>PtRe/CeO₂>Pt/ZrO₂>Pt/CeZrO₂>Pt/CeO₂ showing that activities have been increasing with increasing reducibility of the supported metals [21].

It was detected that the selectivities towards the products (Table 7) did not change with the increasing MeOH conversions before reaching the steady state showing that all products are formed with the constant rates. This fact allowed us to compare product distribution at different conversion levels. The selectivities towards hydrogen were ranging from 74 % to 77 % over all tested materials except Ni/25CeZr where

slightly lower selectivity towards hydrogen (72.7 %) was caused by higher formation of methane. Therefore, hydrogen efficiencies were observed to be directly proportional to MeOH conversions.

Hydrogen production rate, and yields of products obtained in APR of methanol over tested Ni modified catalyst are shown in Supplementary material (Section S4., Table S2).

Table 7. Methanol conversions, hydrogen efficiency, and selectivities toward products over tested catalysts obtained in APR of methanol over tested Ni modified catalyst on various supports in steady state.

Support	X _{MeOH} (%)	E _{H₂} (%)	S _{H₂} (%)	S _{CO} (%)	S _{CO₂} (%)	S _{CH₄} (%)
Zr	26.4	16.3	77.0	4.7	16.7	1.5
17Ce-Zr	50.9	34.3	74.8	5.2	17.8	2.2
25Ce-Zr	58.8	40.9	72.7	5.9	18.0	3.3
17Ce-5La-Zr	45.7	34.4	75.8	3.5	18.6	2.0
10La-Zr	46.6	34.7	74.2	5.2	17.9	2.6
Ce	16.9	7.3	75.7	15.6	8.6	0.0

In order to achieve high hydrogen production, high activity in the reforming reaction should be accompanied by high activity in WGS. Evaluation of WGS is primarily expressed as a ratio of CO₂ to CO (Fig. 5). Furthermore, ratio of CO₂ to sum of CO and CH₄ comparing WGS activity to activities of undesired competitive methane formation, causing decrease of H₂ production, is depicted in Fig. 5. The highest WGS activity was achieved over Ni/17Ce-5La-Zr, which led to the comparable H₂ production efficiency as Ni/17Ce-Zr but at lower MeOH conversion. On the other hand, the lowest WGS activity, leading to higher yield of CO than CO₂, was observed in case of using pure CeO₂ as a support. All other supports showed similar ratio of CO₂ to CO production, being over 3 (mol/mol). The highest WGS activity of 17Ce-5La-Zr correlates with its highest basicity among the studied catalysts (See section 3.1.6) since it has been proven previously that presence of basic sites on the catalysts surface is preferred for high WGS activity [42].

WGS is reversible mildly exothermic reaction which should result to almost total conversion of CO to CO₂ under conditions used in APR [43]. Therefore, it can be concluded that equilibrium concentrations were not achieved.

It has been published previously that the ceria-supported catalysts generally show very high activity in WGS reactions because of high oxygen storage capacity of those materials [10,11]. On the other hand, those conclusions were drawn once WGS had been tested in gas-phase system. High WGS activity in APR of ethanol for Ni supported on CeO₂ has been presented by Roy et al. [12]. However, very low conversions of ethanol up to 6 % have been achieved because of different reaction conditions as lower reaction temperature (175 °C) and lower pressure (14-28 bar) were used [12]. As a contrast, Lee et al. detected very high selectivity towards CO over 15 wt-% Ni/CeO₂ in APR of glycerol performed at 250 °C [24] which is in consistence with current results.

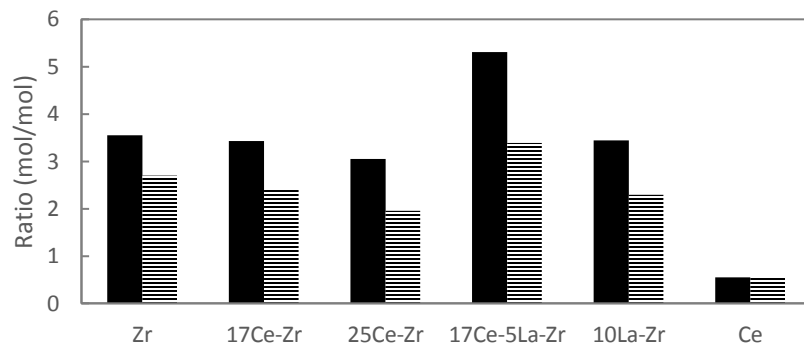


Figure 5. Evaluation of WGS activity as a function of ratio of CO₂ to CO (solid) and CO₂ to sum of CO and CH₄ (line).

3.2.1 Catalysts stability

The possibility of the catalyst reuse after their re-reduction in the APR reaction was tested for all catalysts except Ni/Ce, which showed very low activity in the first run.

Methanol conversions as a function of reaction time with the fresh and re-reduced catalysts are compared in Fig. 6. Steady states of the reaction were achieved within 90 minutes from the beginning of MeOH feeding with all fresh as well as re-reduced catalysts (Fig. 6).

When comparing fresh catalysts, only Ni/10La-Zr and Ni/25Ce-Zr showed stable activity with no decrease of MeOH conversion after reaching steady state. Slight deactivation during the experiment, with 5% decrease of MeOH conversion (compared to steady state), was observed using all other catalysts.

Remarkable drop of activities can be seen from comparison of fresh and re-reduced Ni/17Ce-Zr and Ni/25Ce-Zr, suggesting that the sintering of Ni particles causing catalysts deactivation occurred during the reduction step. This fact was already suggested while comparing results obtained by XRD and H₂ chemisorption (Section 3.1.3. and 3.1.4) and is in consistence with results published by Mafro et al. [38].

When comparing re-reduced catalysts, most of the spent catalysts showed stable activity with low decrease of MeOH conversion, being around 3% in exception of Ni/25Ce-Zr where MeOH conversion drop was almost 10 %.

Compared to Ni particles of 11-13 nm (determined by XRD) in the fresh particles, the sintered Ni particles with sizes over 45 nm were determined in all spent catalysts containing Ce in their support lattice causing decrease in the activity of these catalysts (See Table 5). In the contrast, Ni particle size for spent Ni/La-Zr increased only to 34 nm.

As can be seen from Fig. 6, catalyst Ni/La-Zr exhibited the highest stability when comparing steady state values in two subsequent experiments. Decrease of MeOH conversion was determined to be below 4 % since the steady state conversion was 46.3 % and the final conversion after 12 h was 42.7 %. This is in line with the lowest sintering rate of Ni particles on this support.

As a result of all listed deactivations, comparable conversions of MeOH after 12 h on stream (two subsequent APR experiments à 6 h) conversions (39-43 %) were achieved over all tested mixed oxide supported catalysts.

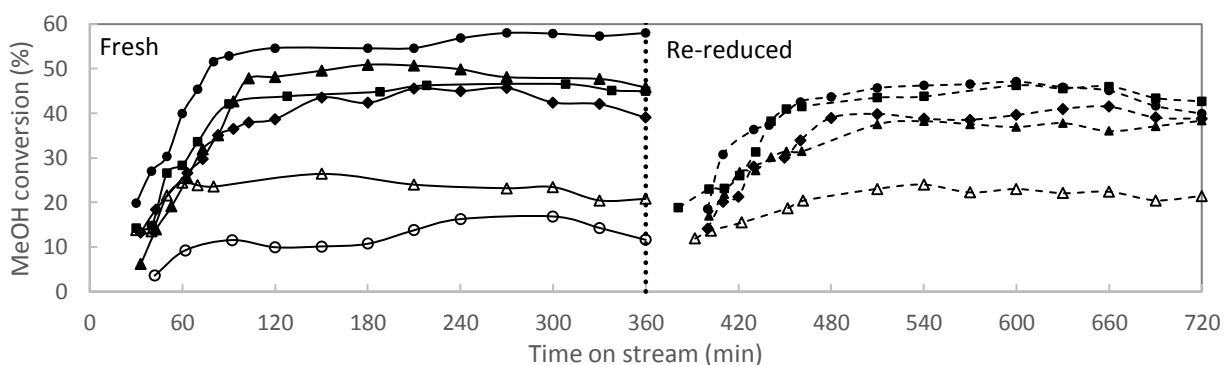


Figure 6. Conversion of methanol as a function of reaction time over fresh (solid line) and re-reduced (dashed line) catalysts: Ni/Zr (Δ), Ni/17Ce-Zr (\blacktriangle), Ni/25Ce-Zr (\bullet), Ni/17Ce-5La-Zr (\blacklozenge), Ni/10La-Zr (\blacksquare) and Ni/Ce (\circ). **Note:** Catalysts re-reduction after 360 min.

The selectivities towards the products listed in Table 8 obtained over re-reduced catalysts did not change with the increasing MeOH conversions as in case of using fresh catalysts. The selectivities towards hydrogen were also ranging from 74 % to 77 % over all the tested materials as in case of fresh catalyst showing that overall deactivation of the materials do not influence H₂ formation.

Comparing selectivities to CO₂ and CO over spent and fresh catalyst, some decrease in WGS activity was observed in case of Ni/Zr and Ni/17Ce-Zr since the selectivity toward CO increased while selectivity toward CO₂ decreased. On the other hand, WGS activity seems to be rather comparable with all other materials and the highest CO₂ to CO ratio was again determined for Ni/17Ce-5La-Zr corresponding with its highest basicity.

The lower amount of methane was formed over all re-reduced catalyst in exception of Ni/La-Zr where CH₄ yield remained the same as in the case of using the fresh catalysts. This catalyst exhibited the lowest deactivation from the point of MeOH conversion and obviously all sites active in methane formation remained intact as well.

Table 8. Methanol conversion after two subsequent experiments and selectivities towards products over re-reduced Ni catalysts on various supports.

Support	X _{MeOH} (%) [*]	S _{H₂} (%)	S _{CO} (%)	S _{CO₂} (%)	S _{CH₄} (%)
Zr	21.5	76.1	7.8	15.0	1.1
17Ce-Zr	38.3	76.8	6.7	15.8	0.8
25Ce-Zr	39.9	74.9	4.6	18.3	2.1
17Ce-5La-Zr	38.8	76.2	3.3	18.7	1.8
10La-Zr	42.7	74.5	4.2	18.3	3.0

*after 12h on stream

It can be concluded that some deactivation addressed to sintering of Ni particles was observed in case of catalysts tested within the current study. However, deactivation observed over tested catalysts was much lower in comparison with the most catalyst tested in APR studies. It should be emphasized here, that the lattice of supports remained intact and metallic Ni did not undergo change in its oxidation state. Problem with the sintering of Ni particles could be avoided by using different preparation methods, which might lead to the stronger interaction between Ni and support. Other preparation methods improving Ni dispersion and resistance toward sintering can be solution combustion, co-precipitation, sol-gel or some complexing methods [18,19,25,38].

4. Conclusions

Activity of series of nickel catalysts supported on ZrO₂, CeO₂ and La₂O₃ oxide supports were evaluated for hydrogen production via aqueous-phase reforming (APR) of methanol in continuous laboratory scale experiments. Using of mixed oxides of Zr, Ce and La instead of pure oxides of ZrO₂ and CeO₂ as support for Ni was proven highly beneficial for the catalytic activity. The highest hydrogen efficiency representing the hydrogen production compared to theoretical yield of hydrogen, of over 40 % was achieved using the most active catalyst of the study, Ni/25Ce-Zr. The highest WGS activity, which enhance the hydrogen production, was determined for Ni/17Ce-%La-Zr and was confirmed to be in line with the highest basicity of this material.

Slight deactivation of catalysts was observed during either APR experiments or reduction steps and was addressed to Ni particles sintering. Other deactivation processes typical for APR studies, such as leaching of Ni and changes in Ni oxidation state or in the supports lattice were excluded based on results of the various characterization methods, which indicates that the prepared catalyst exhibited very promising stability.

Acknowledgement

This work was funded by the Academy of Finland (Project no. 285398). D.Sc. Sonja Kouva, D.Sc. Tiia Viinikainen and Ms. Heidi Meriö-Talvio are acknowledged for performing and evaluating the CO₂-TPD experiments. The authors would like to thank Prof. Klaus Hellgardt and Prof. Leon Lefferts, members of the scientific advisory board of the AQUACAT project, for their guidance and support. Members of the AQUACAT scientific team, Prof. Juha Lehtonen, D.Sc. Pekka Simell, D.Sc. Matti Reinikainen and M.Sc. Irene Coronado, are acknowledged for cooperation.

References

- [1] G.W. Huber, J.A. Dumesic, An overview of aqueous-phase catalytic processes for production of hydrogen and alkanes in a biorefinery, *Catal. Today*. 111 (2006) 119–132.

- [2] J.W. Shabaker, R.R. Davda, G.W. Huber, R.D. Cortright, J.A. Dumesic, Aqueous-phase reforming of methanol and ethylene glycol over alumina-supported platinum catalysts, *J. Catal.* 215 (2003) 344–352.
- [3] R.D. Cortright, R.R. Davda, J.A. Dumesic, Hydrogen from catalytic reforming of biomass-derived hydrocarbons in liquid water., *Nature.* 418 (2002) 964–967.
- [4] R.R. Davda, J.W. Shabaker, G.W. Huber, R.D. Cortright, J.A. Dumesic, A review of catalytic issues and process conditions for renewable hydrogen and alkanes by aqueous-phase reforming of oxygenated hydrocarbons over supported metal catalysts, *Appl. Catal. B Environ.* 56 (2005) 171–186.
- [5] H. Wikberg, V. Grönberg, J. Jermakka, K. Kempainen, M. Kleen, C. Laine, V. Paasikallio, A. Oasmaa, Hydrothermal refining of biomass — an overview and future perspectives, *Tappi J.* 14 (2015) 195–207.
- [6] I. Coronado, M. Stekrova, M. Reinikainen, P. Simell, L. Lefferts, J. Lehtonen, A review of catalytic aqueous-phase reforming of oxygenated hydrocarbons derived from biorefinery water fractions, *Int. J. Hydrogen Energy.* 41 (2016) 11003–11032.
- [7] P.D.L. Mercera, J.G. Van Ommen, E.B.M. Doesburg, A.J. Burggraaf, J.R.H. Ross, Zirconia as a support for catalysts: evolution of the texture and structure on calcination in air, *Appl. Catal.* 57 (1990) 127–148.
- [8] Y. Han, J. Zhu, Surface science studies on the zirconia-based model catalysts, *Top. Catal.* 56 (2013) 1525–1541.
- [9] G. Nahar, V. Dupont, Hydrogen production from simple alkanes and oxygenated hydrocarbons over ceria-zirconia supported catalysts: Review, *Renew. Sustain. Energy Rev.* 32 (2014) 777–796.
- [10] S. Hilaire, X. Wang, T. Luo, R.J. Gorte, J. Wagner, A comparative study of water-gas-shift reaction over ceria-supported metallic catalysts, *Appl. Catal. A Gen.* 258 (2004) 271–276.
- [11] T. Bunluesin, R.J. Gorte, G.W. Graham, Studies of the water-gas-shift reaction on ceria-supported Pt, Pd, and Rh: Implications for oxygen-storage properties, *Appl. Catal. B Environ.* 15 (1998) 107–114.
- [12] B. Roy, C.A. Leclerc, Study of preparation method and oxidization/reduction effect on the performance of nickel-cerium oxide catalysts for aqueous-phase reforming of ethanol, *J. Power Sources.* 299 (2015) 114–124.
- [13] S.C. Dantas, J.C. Escritori, R.R. Soares, C.E. Hori, Effect of different promoters on Ni/CeZrO₂ catalyst for autothermal reforming and partial oxidation of methane, *Chem. Eng. J.* 156 (2010) 380–387.
- [14] M. Li, Z. Feng, G. Xiong, P. Ying, Q. Xin, C. Li, Phase transformation in the surface region of zirconia detected by UV Raman spectroscopy, *J. Phys. Chem. B.* 105 (2001) 8107–8111.
- [15] H. Kawabata, Y. Koda, H. Sumida, M. Shigetsu, A. Takami, K. Inumaru, Active three-way catalysis of rhodium particles with a low oxidation state maintained under an oxidative atmosphere on a La-containing ZrO₂ support, *Chem. Commun.* 49 (2013) 4015.

- [16] G. Pantaleo, V. La Parola, F. Deganello, P. Calatozzo, R. Bal, A.M. Venezia, Synthesis and support composition effects on CH₄ partial oxidation over Ni-CeLa oxides, *Appl. Catal. B Environ.* 164 (2015) 135–143.
- [17] H.Z. Feng, P.Q. Lan, S.F. Wu, A study on the stability of a NiO-CaO/Al₂O₃ complex catalyst by La₂O₃ modification for hydrogen production, *Int. J. Hydrogen Energy.* 37 (2012) 14161–14166.
- [18] Y. Xue, C. Yan, X. Zhao, S. Huang, C. Guo, Ni/La₂O₃-ZrO₂ catalyst for hydrogen production from steam reforming of acetic acid as a model compound of bio-oil, *Korean J. Chem. Eng.* 34 (2017) 305–313.
- [19] J. Si, G. Liu, J. Liu, L. Zhao, S. Li, Y. Guan, Y. Liu, Ni nanoparticles highly dispersed on ZrO₂ and modified with La₂O₃ for CO methanation, *RSC Adv.* 6 (2016) 12699–12707.
- [20] A.S. Larimi, M. Kazemeini, F. Khorasheh, Applied Catalysis A : General Aqueous phase reforming of glycerol using highly active and stable Pt_{0.05}Ce_xZr_{0.95-x}O₂ ternary solid solution catalysts, *Applied Catal. A, Gen.* 523 (2016) 230–240.
- [21] A. Ciftci, S. Eren, D.A.J.M. Ligthart, E.J.M. Hensen, Platinum-rhenium synergy on reducible oxide supports in aqueous-phase glycerol reforming, *ChemCatChem.* 6 (2014) 1260–1269.
- [22] A. Chen, H. Guo, Y. Song, P. Chen, H. Lou, Recyclable CeO₂-ZrO₂ and CeO₂-TiO₂ mixed oxides based Pt catalyst for aqueous-phase reforming of the low-boiling fraction of bio-oil, *Int. J. Hydrogen Energy.* 42 (2017) 9577–9588.
- [23] S. Jeon, Y. Min, K. Saravanan, G. Young, B. Kim, J. Lee, J. Wook, Aqueous phase reforming of ethylene glycol over bimetallic platinum-cobalt on ceria e zirconia mixed oxide, *Int. J. Hydrogen Energy.* 42 (2017) 9892–9902.
- [24] H.J. Lee, G.S. Shin, Y.C. Kim, Characterization of supported Ni catalysts for aqueous-phase reforming of glycerol, *Korean J. Chem. Eng.* 32 (2015) 1267–1272.
- [25] B. Roy, H. Sullivan, C. a. Leclerc, Aqueous-phase reforming of n-BuOH over Ni/Al₂O₃ and Ni/CeO₂ catalysts, *J. Power Sources.* 196 (2011) 10652–10657.
- [26] M.M. Rahman, T.L. Church, M.F. Variava, A.T. Harris, A.I. Minett, Bimetallic Pt–Ni composites on ceria-doped alumina supports as catalysts in the aqueous-phase reforming of glycerol, *RSC Adv.* 4 (2014) 18951.
- [27] A. Tanksale, C.H. Zhou, J.N. Beltramini, G.Q. Lu, Hydrogen production by aqueous phase reforming of sorbitol using bimetallic Ni-Pt catalysts: Metal support interaction, *J. Incl. Phenom. Macrocycl. Chem.* 65 (2009) 83–88.
- [28] V. Paasilalilio, J. Kihlman, C.A. Sánchez Sánchez, P. Simell, Y. Solantausta, J. Lehtonen, Steam reforming of pyrolysis oil aqueous fraction obtained by one-step fractional condensation, *Int. J. Hydrogen Energy.* 40 (2015) 3149–3157.
- [29] L.P.F.D. Kohler, Gert H. Du Plessis, Francois J. Du Toit, E.L. Koper, T.D. Phillips, J. Van Der Walt, Method of purifying Fischer-Tropsch derived water, US7153393 (2006).
- [30] J.M. Hernández-Enríquez, R. Silva-Rodrigo, R. García-Alamilla, L. Arcelia García-Serrano, B.E.

- Handy, G. Cárdenas-Galindo, A. Cueto-Hernández, Synthesis and Physico-Chemical Characterization of CeO₂/ZrO₂-SO₄²⁻-Mixed Oxides, *Chem. Soc.* 56 (2012) 115–120.
- [31] Y. Li, Y. Cai, X. Xing, N. Chen, D. Deng, Y. Wang, Catalytic activity for CO oxidation of Cu–CeO₂ composite nanoparticles synthesized by a hydrothermal method, *Anal. Methods.* 7 (2015) 3238–3245.
- [32] Y. Liu, D. Li, B. Lin, Y. Sun, X. Zhang, H. Yang, Hydrothermal synthesis of Ni-doped hierarchically porous carbon monoliths for hydrogen storage, *J. Porous Mater.* 22 (2015) 1417–1422.
- [33] J.T. Richardson, R. Scates, M. V. Twigg, X-ray diffraction study of nickel oxide reduction by hydrogen, *Appl. Catal. A Gen.* 246 (2003) 137–150.
- [34] X. Wang, J.A. Rodriguez, J.C. Hanson, D. Gamarra, A. Martínez-Arias, M. Fernández-García, In Situ Studies of the Active Sites for the Water Gas Shift Reaction over Cu–CeO₂ Catalysts: Complex Interaction between Metallic Copper and Oxygen Vacancies of Ceria, *J. Phys. Chem. B.* 110 (2006) 428–434.
- [35] R. Jain, A.S. Poyraz, D.P. Gamliel, J. Valla, S.L. Suib, R. Maric, Comparative study for low temperature water-gas shift reaction on Pt/ceria catalysts: Role of different ceria supports, *Appl. Catal. A Gen.* 507 (2015) 1–13.
- [36] A. Karpenko, R. Leppelt, J. Cai, V. Plzak, A. Chuvilin, U. Kaiser, R.J. Behm, Deactivation of a Au/CeO₂ catalyst during the low-temperature water-gas shift reaction and its reactivation: A combined TEM, XRD, XPS, DRIFTS, and activity study, *J. Catal.* 250 (2007) 139–150.
- [37] F. Hrizi, H. Dhaouadi, F. Touati, Cerium carbonate hydroxide and ceria micro/nanostructures: Synthesis, characterization and electrochemical properties of CeCO₃OH, *Ceram. Int.* 40 (2014) 25–30.
- [38] R.L. Manfro, A.F. Da Costa, N.F.P. Ribeiro, M.M.V.M. Souza, Hydrogen production by aqueous-phase reforming of glycerol over nickel catalysts supported on CeO₂, *Fuel Process. Technol.* 92 (2011) 330–335.
- [39] P. Biswas, D. Kunzru, Steam reforming of ethanol for production of hydrogen over Ni/CeO₂-ZrO₂ catalyst: Effect of support and metal loading, *Int. J. Hydrogen Energy.* 32 (2007) 969–980.
- [40] S. Jeon, H. Ham, Y.-W. Suh, J.W. Bae, Aqueous phase reforming of ethylene glycol on Pt/CeO₂ – ZrO₂: effects of cerium to zirconium molar ratio, *RSC Adv.* 5 (2015) 54806–54815.
- [41] V. García, J.J. Fernández, W. Ruíz, F. Mondragón, A. Moreno, Effect of MgO addition on the basicity of Ni/ZrO₂ and on its catalytic activity in carbon dioxide reforming of methane, *Catal. Commun.* 11 (2009) 240–246.
- [42] Y. Guo, M.U. Azmat, X. Liu, Y. Wang, G. Lu, Effect of support's basic properties on hydrogen production in aqueous-phase reforming of glycerol and correlation between WGS and APR, *Appl. Energy.* 92 (2012) 218–223.
- [43] C. Wheeler, A. Jhalani, E.J. Klein, S. Tummala, L.D. Schmidt, The water-gas-shift reaction at short contact times, *J. Catal.* 223 (2004) 191–199.